Since January 2020 Elsevier has created a COVID-19 resource centre with free information in English and Mandarin on the novel coronavirus COVID-19. The COVID-19 resource centre is hosted on Elsevier Connect, the company's public news and information website.

European Journal of Pharmaceutical Sciences 167 (2021) 106012

Contents lists available at ScienceDirect

European Journal of Pharmaceutical Sciences

journal homepage: www.elsevier.com/locate/ejps

Inhibition of the RNA-dependent RNA Polymerase of the SARS-CoV-2 by Short Peptide Inhibitors

Suyash Pant [a], N.R. Jena [b,*]

[a] Department of Pharmacoinformatics, National Institute of Pharmaceutical Education and Research Kolkata, Maniktala Main Road, 700054, Kolkata, WB, India
[b] Discipline of Natural Sciences, Indian Institute of Information Technology, Design, and Manufacturing, Dumna Airport Road, Jabalpur-482005, India

ARTICLE INFO

Keywords:
SARS-CoV-2
covid-19
RdRp
Antiviral agents
Peptide Inhibitors

ABSTRACT

The rapid proliferation of SARS-CoV-2 in COVID-19 patients has become detrimental to their lives. However, blocking the replication cycle of SARS-CoV-2 will help in suppressing the viral loads in patients, which would ultimately help in the early recovery. To discover such drugs, molecular docking, MD-simulations, and MM/GBSA approaches have been used herein to examine the role of several short ionic peptides in inhibiting the RNA binding site of the RNA-dependent RNA polymerase (RdRp). Out of the 49 tri- and tetrapeptide inhibitors studied, 8 inhibitors were found to bind RdRp strongly as revealed by the docking studies. Among these inhibitors, the Ala1-Arg2-Lys3-Asp4 and Ala1-Lys2-Lys3-Asp4 are found to make the most stable complexes with RdRp and possess the ΔG_{bind} of -17.41 and -14.21 kcal/mol respectively as revealed by the MD and MM/GBSA studies. Hence these peptide inhibitors would be highly potent in inhibiting the activities of RdRp. It is further found that these inhibitors can occupy the positions of the nucleotide triphosphate (NTP) insertion site, thereby inhibiting the replication of the viral genome by obstructing the synthesis of new nucleotides. Structural and energetic comparisons of these inhibitors with Remdesivir and similar nucleotide drugs show that these peptides would be more specific and hence may act as promiscuous antiviral agents against RdRp.

1. Introduction

The transmission of the severe acute respiratory syndrome coronavirus-2 (SARS-CoV-2) from human to human has resulted in the deaths of millions of people worldwide (Ullah et al., 2021; Wang et al., 2020). This pandemic has severely affected the work culture, socio-economical values, and brought human lives to a standstill. Although emergeny uses of vaccines have been permitted to contain the disease, these are not hundred percent efficient, their long-lasting effects are not known, and it may not be helpful for patients suffering from COVID-19. Hence it is of paramount importance to design drugs (Cava et al., 2020; Jena, 2020a; Kadam and Wilson, 2017; Li and De Clercq, 2020; Li et al., 2020; Liu et al., 2020; Pant et al., 2021; Sheahan et al., 2020; Wu et al., 2020; Zhou et al., 2020) that can decrease the viral loads, suppress its rapid transmission, and cure of the disease. Further, as the virus is rapidly mutating to enter into the host cells by evading the natural and induced (by vaccines) immune systems, it is immensely important to facilitate designs of specific drugs. To do so, it is necessary to understand the structures and functions of different viral proteins and their mode of action in the host cells. Fortunately, structures of several key proteins of the SARS-CoV-2 have been solved now (Astuti and Ysrafil, 2020; Buchholz et al., 2004; da Silva et al., 2020; Gao et al., 2020; Lan et al., 2020; Snijder et al., 2016; Walls et al., 2020; Yin et al., 2020). Among these proteins, the RNA-dependent RNA polymerase (RdRp) was shown to assist in the replication of the viral genome (single-stranded RNA) and was found to be mainly responsible for the proliferation of the virus into different cells (Gao et al., 2020; Snijder et al., 2016; Yin et al., 2020). As the RdRp multiplies viral genomes by synthesizing new RNA nucleotides, its inhibition is essential to control the proliferation of the infection in human cells and hence to control the viral loads in patients.

The recent Cryo-EM structure of the RdRp suggests that the RNA binding site is clamped between the Finger, Palm, and Thumb domains, consisting of several positive (Lys545, Lys551, Arg553, Arg555, Lys593, Arg621, Arg631, etc.) and negative amino acids (Asp618, Asp623, Asp760, Asp761, etc.) as illustrated in Fig. 1 (Yin et al., 2020). These residues play crucial roles in the placement of the RNA, elongation of the RNA strand, and catalysis. Two magnesium ions found at the binding site were also proposed to play a key role in the catalysis. The insertion of new nucleotides into the RNA strand (referred to as the nucleotide

* Corresponding author.
E-mail address: nrjena@iiitdmj.ac.in (N.R. Jena).

https://doi.org/10.1016/j.ejps.2021.106012
Received 9 June 2021; Received in revised form 23 August 2021; Accepted 15 September 2021
Available online 17 September 2021

triphosphate (NTP) insertion site) was also proposed to be assisted by some of these residues (Yin et al., 2020). The insertions of antiviral nucleotide drugs, such as Remdesivir (Yin et al., 2020), Favipiravir (Sada et al., 2020), Molnupiravir (Gordon et al., 2021), and Ribavirin (Bylehn et al., 2021), were also found to be assisted by these residues. Recently, the possible roles of several unnatural nucleotides in inhibiting the activities of RdRp were evaluated (Jena et al., 2021). It was proposed that both the positive and negative amino acids, in particular Lys545, Lys551, Arg553, Arg555, Asp760, and Asp761 play a major role in identifying the inhibitor.

It should be mentioned that as the nucleotide drugs possess modified base and sugar groups, they can inhibit the replication of the virus by employing either a chain termination (Jena et al., 2021; Yin et al., 2020) or a base-pair mutation mechanism (Gordon et al., 2021; Jena, 2020b, 2021). However, these mechanisms do not inhibit the replication immediately; instead, allow a few nucleotides to be inserted into the RNA strand beyond the insertion site of the drug before eventually stalling the replication (Gordon et al., 2020; Jena, 2021). Further, these nucleotide drugs may undergo structural alterations, such as tautomerization, protonation, deprotonation, etc., before or after binding to their targets (Jena, 2020b). This may eventually influence their activity. Recently, it is discovered that the N-terminal ExoN domain of the viral non-structural protein 14 (NSP14) follows an intriguing reaction mechanism in which it rectifies and removes the nucleotide drugs by considering these as replication errors (Liu et al., 2021). Therefore, it is necessary to design alternative inhibitors that can not only immediately block the replication of the virus by interfering with the functioning of RdRp but also provide long-term effects and are safe for humans.

Due to the above reasons, the inhibition of the RdRp activities is studied herein by designing tri- and tetra- ionic peptide inhibitors (Tables S1 and S2, Supporting Information). As peptide inhibitors are less toxic, highly specific, and easy to synthesize, these are attractive alternatives to small-molecule repurposed drugs (Schutz et al., 2020). The short peptides are also less prone to proteolytic cleavage and hence are quite useful against viral diseases (Schutz et al., 2020). More importantly, these inhibitors will not be considered as replication errors like the nucleotide drugs and hence there would be no antiviral resistance to the peptide drugs by replicative enzymes. For these reasons, short ionic peptides and peptidomimetics were used to inhibit different flaviviruses including Zika (Phoo et al., 2018), West Nile (Nitsche et al., 2017), and Dengu viruses (Noble et al., 2012). Peptide inhibitors were also found to be effective against HIV (Gomara et al., 2020). Interestingly, several antiviral peptides were recently shown to inhibit the S-protein of the SARS-CoV-2 (Schutz et al., 2020) (Chowdhury et al., 2020).

2. Computational Methodology

2.1. System Preparation

The structures of the RdRp and two Mg^{+2} ions were extracted from the complex structure, where it was bound to nsp7, nsp8, RNA, and Remdesivir monophosphate (RMP) as deposited in the protein data bank (PDB ID 7BV2) (Yin et al., 2020). The three-dimensional structures of various tri-and tetrapeptides were generated by using the Pymol program (Schrödinger, 2015). The Chimera program (Morris et al., 2007) was used to minimize these peptides for 100 steps by using the steepest descent and conjugate gradient algorithm each. Subsequently, hydrogen atoms were added to these peptides by the GOLD docking program (Hartshorn et al., 2007; Jones et al., 1997; Nissink et al., 2002; Sapundzhi et al., 2019). Before docking, hydrogen atoms were also added to the RdRp by using the UCSF Chimera program) by maintaining the neutral pH. It should be mentioned that as the Lys545 and Arg555 (Fig. 1B) interact with the +1 base of the incoming RNA-strand, which is important for the correct placement of the incoming nucleotide (Yin et al., 2020), it is necessary to block these residues by an inhibitor so that these residues are not available to interact with the viral RNA. Similarly, as the two Mg^{+2} ions coordinated by Asp760 and Asp761 help in the catalysis, these ions and residues should also be blocked by the inhibitor. Keeping this in mind, various peptide inhibitors were modeled that contain charged residues at the N- and C-terminals to make salt-bridge interactions with these and other residues present at the active site (Fig. 1B). In some cases, the N-terminal contains alanine (Ala) to allow the peptides to make some additional interactions (e.g. hydrogen bonds). This procedure generated 49 peptides of varying sequences as presented in Tables S1 and S2 (Supporting Information).

2.2. Molecular Docking

Recently, the performance of different docking algorithms in generating accurate protein-peptide complex structures was analyzed by using 185 experimentally determined protein-peptide complexes. The length of these peptides was varying from 5 to 20 residues (Weng et al., 2020). In this benchmark study, 14 docking programs involving (1) eight protein-peptide docking programs, such as GalaxyPepDock, MDockPeP, HPEPDOCK, CABS-dock, pepATTRACT, DINC, AutoDock CrankPep (ADCP), and HADDOCK, (2) three protein-protein docking programs, such as ZDOCK, FRODOCK, and HawkDock, and (3) three small molecule docking programs, such as GOLD, Surflex-Dock, and AutoDock Vina were used (Sapundzhi et al., 2019). It was found that the performance of GOLD on protein-peptide docking for a known binding site is superior to many other small molecule and protein-protein

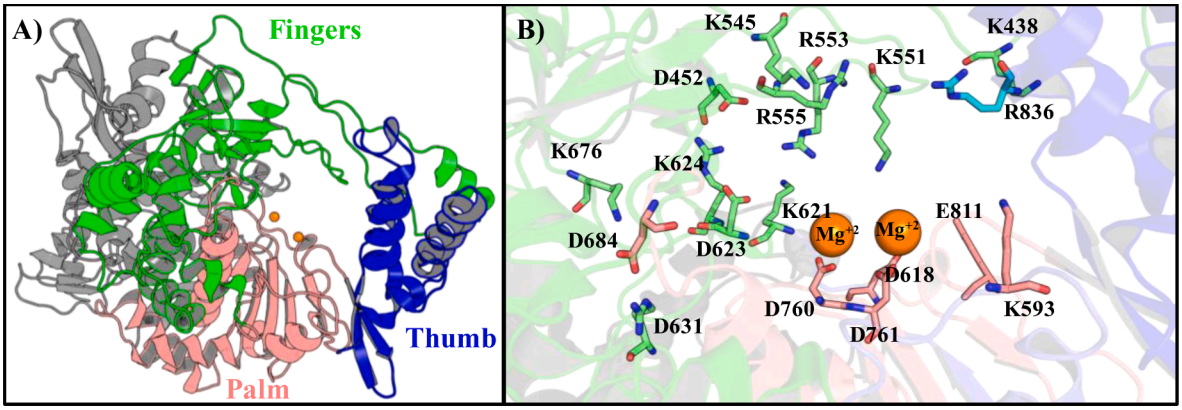

Fig. 1. A) The important domains, such as the Finger (residues 397-581 and 621-679, green color), Palm (residues 582-620 and 680-815, pink color), and Thumb (residues 816-920, blue color) of RdRp (Yin et al., 2020). B) The important ionic residues and Mg^{+2} ions (in the sphere representation) located at the active site of RdRp (PDB ID 7BV2) (Yin et al., 2020).

docking algorithms (Weng et al., 2020). The genetic algorithm implemented in GOLD was also found to possess the best sampling power (Weng et al., 2020). However, for proteins, where the binding site is not known, HPEPDOCK was found to be the best docking program. As we were intended to find the poses for the known binding site of RdRp, GOLD is believed to produce accurate peptide-bound protein conformations.

To validate the sampling power of GOLD, coordinates of Lys-Lys-Arg (PDB ID 5ZMQ) (Phoo et al., 2018) and Arg-Arg-Arg (PDB ID 5ZOB) (Phoo et al., 2018) bound to the NS3-NS2B protease of the Zika virus were extracted from their experimental complex structures to dock them into the binding site of the protease. It should be mentioned that these peptides were connected to small inorganic molecules at the C- and N-terminals, which were deleted before docking. As evident from Fig. 2, the use of the Chemscore function of the GOLD program satisfactorily reproduced the experimental binding modes of the protein-peptide complexes (Phoo et al., 2018). The superimpositions of docked conformations of Lys-Lys-Arg and Arg-Arg-Arg peptide-protein complexes onto the corresponding experimental structures by considering the C_α atoms produced the root mean square deviations (RMSD) of 0.3 Å and 0.03 Å respectively. These results underline the accuracy of the GOLD program in producing reliable protein-peptide conformations.

In an earlier study, the power of different docking algorithms in predicting (1) accurate binding affinity (scoring power), (2) binding pose (docking power), (3) true binders from random molecules (screening power), and (4) relative ranking (ranking power), about 20 scoring functions were evaluated (Li et al., 2014). It was found that Chemscore function of GOLD has good docking power and ChemPLP function has good scoring, screening, and ranking powers (Li et al., 2014). Therefore, it is believed that the use of Chemscore for docking and ChemPLP for scoring and ranking can provide accurate results (Li et al., 2014).

For the above reasons, molecular dockings of various peptides into the active site of the RdRp-Mg^{+2} complex were carried out by using the Chemscore function of GOLD 5.0 program (Hartshorn et al., 2007; Jones et al., 1997; Nissink et al., 2002; Sapundzhi et al., 2019). The scoring and ranking of docked poses were carried out by using the ChemPLP function (Hartshorn et al., 2007; Jones et al., 1997; Nissink et al., 2002; Sapundzhi et al., 2019). The genetic algorithm (Sapundzhi et al., 2019) was used for docking purposes to create ten different conformations of each peptide by keeping the protein rigid. The binding site was considered to be situated within a radius of 10Å from Asp623 . Out of the ten different poses, the one which makes the most ionic and hydrogen-bonding interactions with the charged amino acids and possesses the highest docking score was shortlisted. The short-listed poses were about 10-12 kcal/mol more stable than the second most stable pose. Further, each short-listed conformation of the peptide was populated most of the time during the docking (5-6 times out of 10 poses) with slight fluctuations in the orientation of the side chains. Additionally, in these peptides, the Asp residue was making ionic interactions with the Mg^{+2} ions like the PO_4-Mg^{+2} interactions in the case of nucleotide drugs. Hence, it is believed that the short-listed peptides would be bioactive. The details of the short-listed peptides, such as docking scores, the amino acid residues of RdRp with which they are making interactions, etc. are presented in Tables S1 and S2. From these Tables, it is evident that two tripeptides namely Arg1-Arg2-Asp3, (peptide 1), and Lys1-Lys2-Asp3, (peptide 2), and six tetrapeptides, such as Ala1-Arg2-Arg3-Asp4 (peptide 3), Ala1-Lys2-Lys3-Asp4 (peptide 4), Ala1-Arg2-Lys3-Asp4 (peptide 5), Ala1-Lys2-Arg3-Asp4 (peptide 6), Arg1-Arg2-Asp3-Asp4 (peptide 7), and Asp1-Asp2-Arg3-Lys4 (peptide 8) have docking scores more than 80 kcal/mol. Therefore, these 8 peptides were shortlisted for subsequent molecular dynamics (MD) studies.

2.3. Molecular Dynamics Simulations

To gain deeper insights into the binding modes of the above eight peptide inhibitors with RdRp, each peptide-RdRp complex was subjected to MD simulations. As the Cryo-EM structure does not account for the dynamical and solvation effects of the protein and the protein was held rigid during docking, it was necessary to understand the roles of protein dynamics on the binding of peptide inhibitors. The molecular dynamics simulations were undertaken by using the Desmond 2018-4 package of the Schrodinger (2006; Bowers et al., 2006b). The detailed protocol used for the simulations is the same as employed earlier (Gahtori et al., 2020; Jena et al., 2021). In short, initially, the protein-inhibitor complexes were solvated by placing them in an explicit water box of size 10 Å. The OPLS3e force field (Roos et al., 2019) was

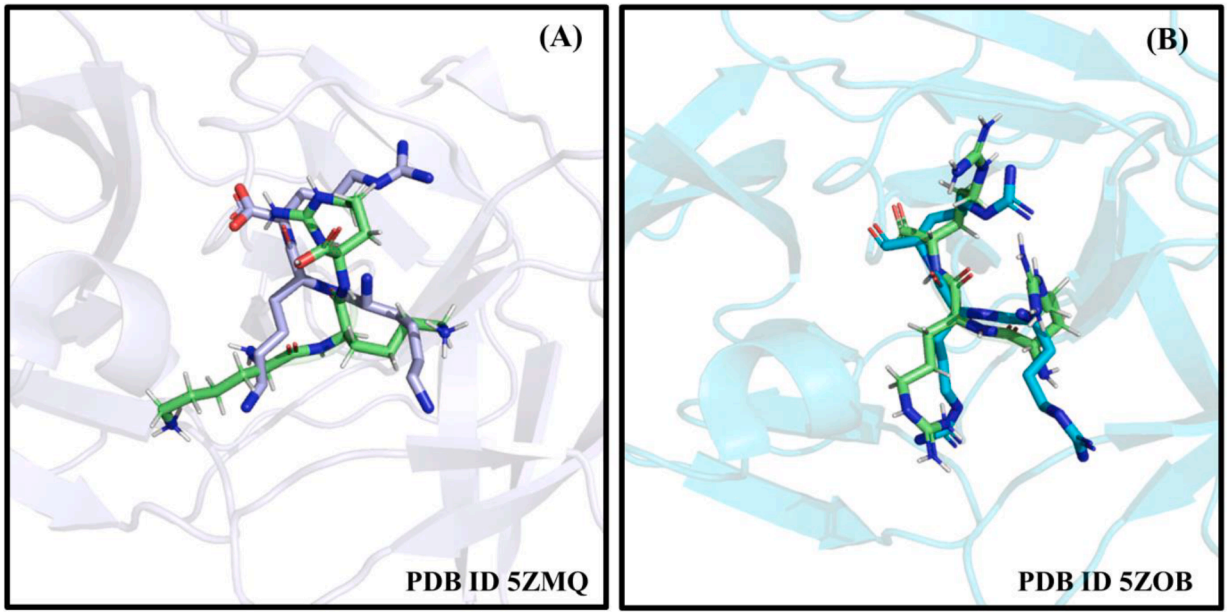

Fig. 2. Molecular docking of (A) Lys-Lys-Arg (in lime color) and (B) Arg-Arg-Arg (in lime color) into the binding site of the NS2B-NS3 protease of the Zika Virus by using the Chemscore function of GOLD. This shows that the experimental binding modes (in light blue color in (A) and cyan color in (B)) can be satisfactorily reproduced by the GOLD program.

used to model the protein and peptide inhibitors, while the single-point charge (SPC) model (Berendsen et al., 1987) was used to account for the explicit water molecules. Sufficient numbers of ions were added to make the solvated complexes neutral. The protonation states of the protein and peptide residues were set as per the pH=7.0. Subsequently, these complexes were energy minimized 2000 steps by using each of the steepest descent and limited-memory Broyden--Fletcher-Goldfarb-Shanno (LBFGS) algorithm. The minimized complexes were slowly heated to maintain a temperature of 300 kelvin (K) in several steps by using the Nose-Hoover thermostatic algorithm (Posch et al., 1986). In the first step, the system was heated to 10 K for 100 ps to reduce any possible steric clashes. In the second step, a 12 ps of molecular dynamics run was performed with the NVT ensemble to relax the system at 10 K. In the third step, molecular dynamics run of 12 ps was carried out by using the NPT ensemble, where a pressure of 1 atm was maintained by using the Langevin barostat (Martyna et al., 1994). In the fourth step, the temperature was raised to 300 K for 12 ps by using the NPT ensemble. In all of the above steps, the solute heavy atoms were restrained with a force constant of 50 kcal $mol^{-1}Å^{-1}$. In the fifth step, restraint was released and the molecular dynamics simulation was carried out at NPT ensemble for 24 ps. Subsequently, the system was subjected to a production run for 200 ns by considering the integration time step of 1 fs and the NPT ensemble. It should be mentioned that a 200 ns time scale was chosen to allow each complex to properly equilibrate and produce biologically meaningful results. As most of the biologically relevant motions occur on the microsecond to the millisecond time scale, which is computationally expensive to achieve, it is necessary to simulate systems for a longer time depending on the computational facilities available. The periodic boundary condition (PBC) was considered for all of the simulations. The simulation interaction diagram tool implemented in the Desmond 2018-4 package (Bowers et al., 2006a) was used to analyze the detailed interactions between the protein and peptide inhibitors.

To calculate the relative binding free energies of each RdRp-peptide complex, the MM-GBSA technique was used. For this purpose, 500 snapshots were considered from the last 50 ns trajectories of the MD simulations at an interval of 100 ps. Equation (1) was used to compute the relative binding free energy.

$$\Delta G_{bind} = G_{complex\ (minimized)} - G_{protein\ (unbound,\ minimized)} - G_{ligand\ (unbound,\ minimized)} \quad ----(1)$$

where, ΔG_{bind} is the calculated relative binding free energy, $G_{complex\ (minimized)}$ is the MM/GBSA energy of the minimized complex, $G_{protein\ (unbound,\ minimized)}$ is the MM/GBSA energy of the minimized protein after separating it from its bound ligand and $G_{lig\ (unbound,\ minimized)}$ is the MM/GBSA energy of the ligand after separating it from the complex and allowing it to relax. However, as entropy calculations were not performed, the free energy terms contain contributions from the enthalpy terms only.

3. Results and Discussions

3.1. The Binding of Tripeptides to RdRp

Among the different tripeptides studied here, peptides 1 and 2 are associated with the highest docking scores (higher binding affinity) (Table S1). Among these two peptides, the docking score of peptide 1 is higher than that of peptide 2. This indicates that the former peptide may bind strongly with RdRp. However, consideration of protein dynamics and solvation effects may alter the binding preferences of these peptides. Therefore, we will only discuss the binding modes of these two and other peptides as obtained by the MD simulations. Interested readers may refer to Figs. S1-S4 and Tables S1 and S2 (Supporting Information) for the detailed interactions of the peptides with RdRp as revealed by the docking studies. It should be mentioned that MD-simulations produced quite stable complexes as can be found from Figs. 3 and 4. From Fig. 3, it is evident that all of the complexes had a root mean square deviation (RMSD) of the C_α atoms less than 2.5 Å computed with respect to the corresponding minimized structures. Similarly, the root mean square fluctuations of the protein residues are also found to be normal (Fig. 4). These results indicate that not only protein-peptide complexes were properly equilibrated but also produced stable complexes.

To understand the detailed interactions of the tripeptide inhibitors with different residues of RdRp throughout the simulations, the average simulated complex structures are shown in Fig. 5 and a timeline representation of the various interactions (hydrogen bonding, hydrophobic, ionic, water bridges, etc.) and total numbers of peptide-protein contacts are depicted in Fig. S5. The relative binding free energies (ΔG_{bind}) (kcal/mol) of these complexes are presented in Table 1. The standard deviation in ΔG_{bind} is also presented in this table. The variations of ΔG_{bind} with respect to the last 50ns of simulations are shown in Fig. S6. The 2D-diagrams showing percentage occupations of different interactions between tripeptide inhibitors and RdRp are shown in Fig. S7.

3.1.1. The Binding Mode and Stability of Peptide 1 (Arg1-Arg2-Asp3)

The placement of peptide 1 into the binding cavity of RdRp and the comparison of structural alterations before and after simulations are shown in Fig. 5A. The detailed protein-peptide 1 direct and indirect (water-mediated) interactions are depicted in Figs. 5B and S7A. The most stable protein-peptide direct interactions that lasted for more than 50% of the simulation time are presented in Table 2.

As illustrated in Fig. 5A, except for Arg1, which moves downward,

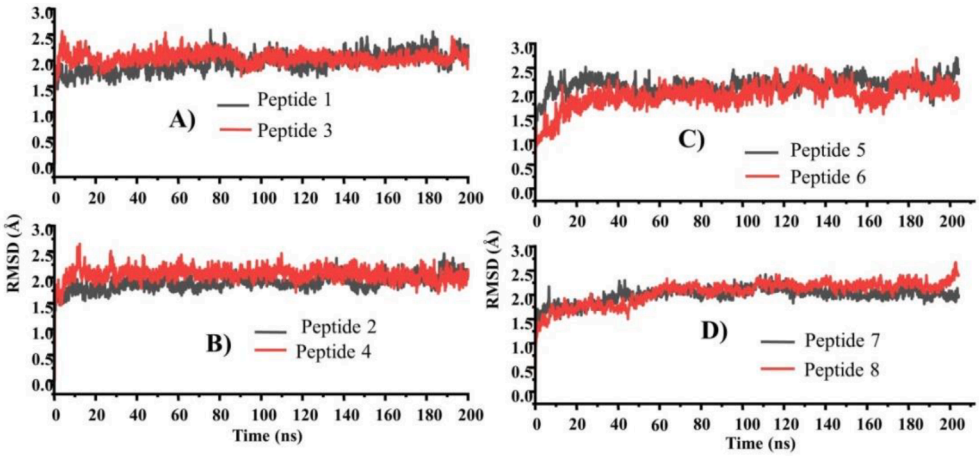

Fig. 3. The variations of the root mean square deviations (RMSD) of the C_α atoms of the protein with time. The RMSD of each complex was computed with respect to the corresponding minimized structure.

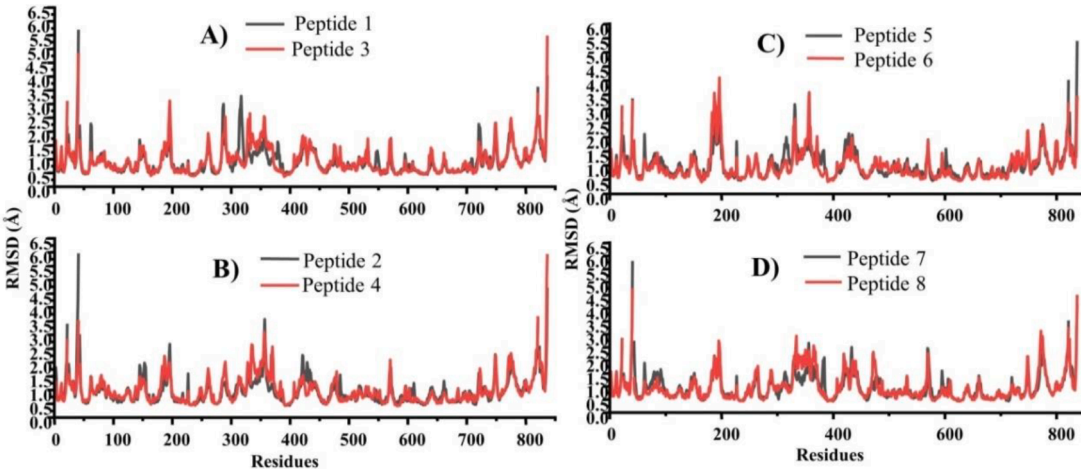

Fig. 4. The variations of the root mean square fluctuations (RMSF) of the different residues of the protein with time. The RMSF of each complex was computed with respect to the corresponding minimized structure.

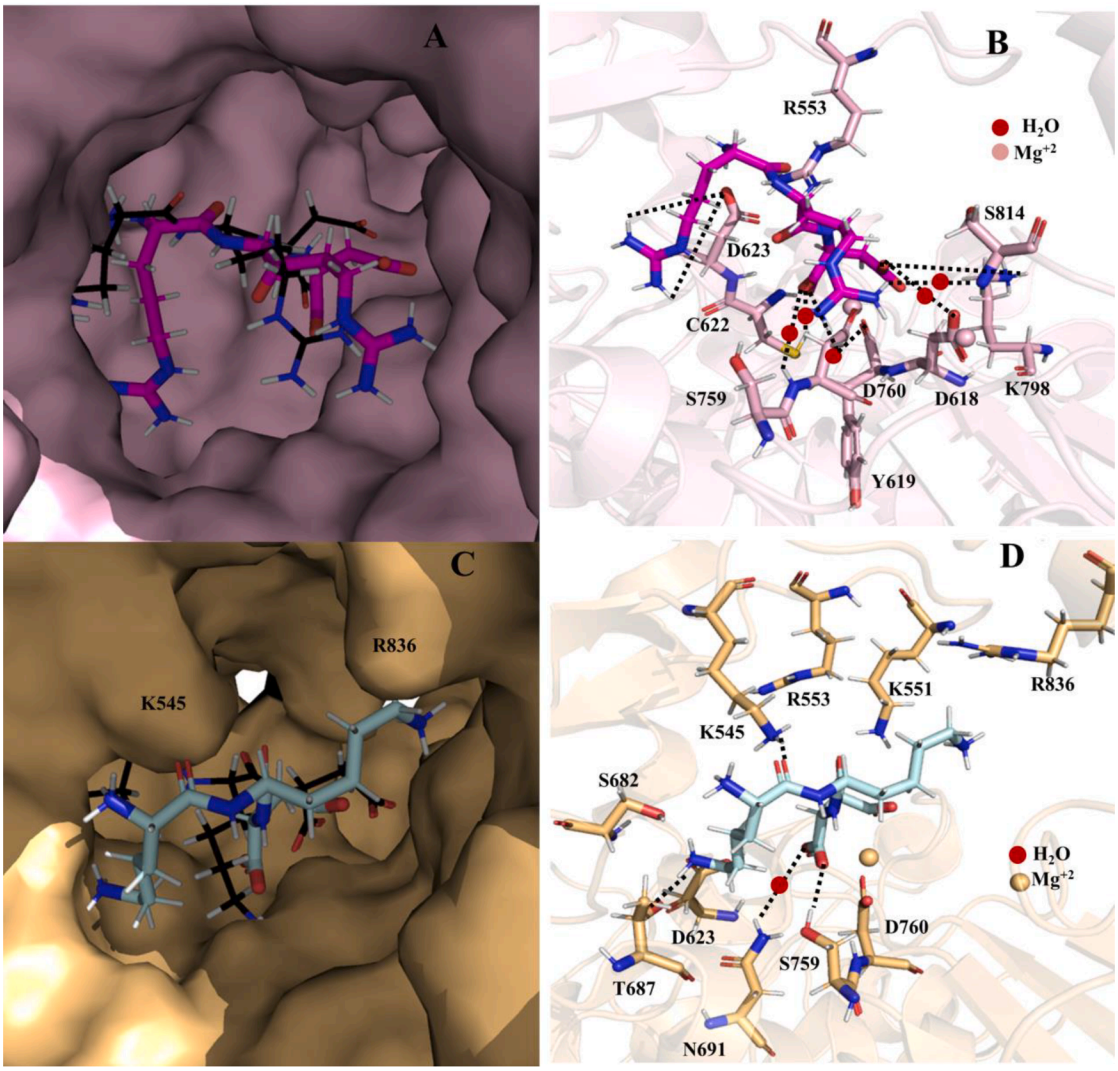

Fig. 5. The comparison of simulated (in magenta color) and docked (in black color) conformations of peptide 1 in the active site of the RdRp (surface representation, in light pink color). (B) The average simulated structure of peptide-1-RdRp complex and their various interactions. (C) The comparison of simulated (in pale cyan color) and docked (in black color) conformations of peptide 2 in the active site of the RdRp (surface representation, in orange color). D) The average simulated structure of peptide-2-RdRp complex and their various interactions.

Table 1
The comparison of ChemPLP docking fitness (kcal/mol) and MM/GBSA average relative total binding free energies (ΔG_{bind}) (kcal/mol) of different peptide inhibitors. Standard deviation (SDV) of binding free energies is also shown.

Peptide	Peptide 1	Peptide 2	Peptide 3	Peptide 4	Peptide 5	Peptide 6	Peptide 7	Peptide 8
Docking Score	90.09	80.83	87.47	80.17	75.84	85.90	85.56	86.95
ΔG_{bind}	10.18	10.42	13.77	-14.21	-17.41	-6.28	-10.72	-10.12
SDV	9.64	4.20	5.85	6.52	7.32	6.30	7.04	3.94

Peptide 1=Arg1-Arg2-Asp3, Peptide 2=Lys1-Lys2-Asp3, Peptide 3=Ala1-Arg2-Arg3-Asp4, Peptide 4=Ala1-Lys2-Lys3-Asp4, Peptide 5=Ala1-Arg2-lys3-Asp4, Peptide 6=Ala1-Lys2-Arg3-Asp4, Peptide 7=Arg1-Arg2-Asp3-Asp4, Peptide 8= Asp1-Asp2-Arg3-Lys4.

Table 2
A list of various protein-peptide interactions that lasted for more than 50% of the simulation time.

Complexes	Interactions
RdRp—Peptide 1	Mg^{+2}—Asp3
RdRp—Peptide 2	Asp623—Lys1 Mg^{+2}—Asp3
RdRp—Peptide 3	Thr680—Ala1 Asp623—Ala1 Ala558—Ala1 Cys622—Asp4 Mg^{+2}—Asp4
RdRp—Peptide 4	Asp623—Ala1 Ser682—Ala1 Thr680—Ala1 Cys622—Lys2 Mg^{+2}—Asp4
RdRp—Peptide 5	Asp623—Arg2 Mg^{+2}—Asp4
RdRp—Peptide 6	Asp623—Ala1 Thr687—Ala1 Asp623—Arg3 Cys622—Asp4 Mg^{+2}—Asp4
RdRp—Peptide 7	Asp623—Arg1 Asp623—Arg2 Mg^{+2}—Asp4
RdRp—Peptide 8	Asp618—Asp1 Mg^{+2}—Asp1

other residues of peptide 1 do not change much from their initial docking conformation. It is found that Arg1 makes a salt-bridge (38% occupancy) and two hydrogen-bonding interactions with Asp623 (42% and 58% occupancies) (Figs. 5B, S7A). Similarly, the side chain and carbonyl backbone atoms of Arg2 are making hydrogen bonds with Ser682 (45% occupancy) and Arg553 (36% occupancy) respectively. Asp3 is found to make an ionic interaction with one of the Mg^{+2} ions that lasted 100% of simulation time (Figs. 5B, S7A). It is also found to make several water-mediated hydrogen bonds with Asp618, Tyr619, Cys622, Asp623, Ser759, and Lys798 (Fig. 5B). Other than these, it may interact with other residues for a lesser time during the simulation (Fig. S5A). However, except Asp3-Mg^{+2} electrostatic interactions, all other interactions are transient and lasted for less than 50% of the simulation time (Table 2). Due to this reason, a positive ΔG_{bind} of about 10.18 kcal/mol is obtained for peptide 1-RdRp complex (Table 1). This indicates that the binding of peptide 1 to RdRp would not be strong.

3.1.2. The Binding Mode and Stability of Peptide 2 (Lys1-Lys2-Asp3)

During the simulations, Peptide 2 undergoes a significant structural reorientation from its original docked conformation (Fig. 5C). Lys1 moved downward toward the Palm domain, whereas Lys2 positioned itself between the Palm and Thumb domains (Fig. 5C). This reorientation helped Lys1 to make a strong ionic interaction with Asp623 (78% occupancy) and a weak hydrogen bond with Thr687 (39% occupancy) (Figs. 5D, S7B). The backbone carbonyl group of Lys2 makes a weak hydrogen bond with Lys545 (39% occupancy). Similarly, Asp3 makes a strong ionic interaction with one of the Mg^{+2} ions (100% occupancy) and a weak hydrogen bond with Ser759 (48% occupancy) (Figs. 5D, S7B). Other than these, it can make water-mediated hydrogen bonds with Asn691 and Asp623 (Figs. 5D, S7B). It can also interact with other residues although for a lesser time during the simulations (Fig. S5B). Despite of these interactions, a positive ΔG_{bind} of about 10.42 kcal/mol is obtained for the peptide 2-RdRp complex (Table 1). This is mainly because of the unfavorable Coulombic interactions between Lys2 and Lys551 and between Lys2 and Arg836 (Fig. 5C,D). If we compare the total number of interactions made by peptides 1 and 2 with RdRp, it is clear that the former peptide binds slightly more tightly with RdRp than that of the latter (Figs S5A and S5B).

3.2. The Binding of Tetrapeptides to RdRp

Among the six tetrapeptides considered for MD-simulations, peptides 3 and 4 are the N-terminal extensions of peptides 1 and 2 respectively. Similarly, peptides 5 and 6 are derived from peptide 4 by mutating its 2^{nd} and 3^{rd} residues respectively. However, peptides 7 and 8 have completely different sequences without any similarity with peptides 1-6. To understand the detailed binding modes of these peptides, the average simulated structures of peptide-RdRp complexes are depicted in Figs. 6-8. A time-line representation of various interactions and total number of protein-peptide contacts obtained during the 200ns simulations are illustrated in Figs. S8-S10. A 2D-interaction diagram showing important interactions that lasted for more than 30% of the simulation time are shown in Figs. S11-S13.

3.2.1. The Binding Mode and Stability of Peptide 3 (Ala1-Arg2-Arg3-Asp4)

In going from the docked to the simulated conformations, Arg3 of peptide 3 moved upward and the overall conformation remained similar to the original one (docked conformation) (Fig. 6A). In the simulated complex, the terminal NH_3^+ group of Ala1 makes an ionic interaction with Asp623 (30% occupancy) and a hydrogen bond with Thr680 (59% occupancy) (Figs. 6B, S11A). Its amide and carbonyl backbone atoms are also making strong hydrogen bonds with Asp623 (86% occupancy) and Ala558 (60% occupancy) respectively (Figs. 6B, S11A). Similarly, Arg2 makes two water-mediated indirect hydrogen bonds with Cys622 and Thr680, while Arg3 makes a water-mediated hydrogen bond with Ile548 (Figs. 6B, S11A). The Asp4 makes a strong ionic interaction with one of the Mg^{+2} ions (100% occupancy) and a strong hydrogen bond with Cys622 (76% occupancy) (Figs. 6B, S11A). It also makes a few water-mediated hydrogen bonds with Asn691, Ser759, and Asp760, (Figs. 6B, S11A). In addition to the above residues, it may interact with various other residues as depicted in Fig. S8A. However, although peptide 3 makes 5 strong interactions with RdRp (Table 2), a ΔG_{bind} of about 13.77 kcal/mol is obtained for the peptide 3-RdRp complex (Table 1). This is because the orientation of peptide 3 is such that Arg3 falls in the cleft formed between Arg553 and Arg836. This generates

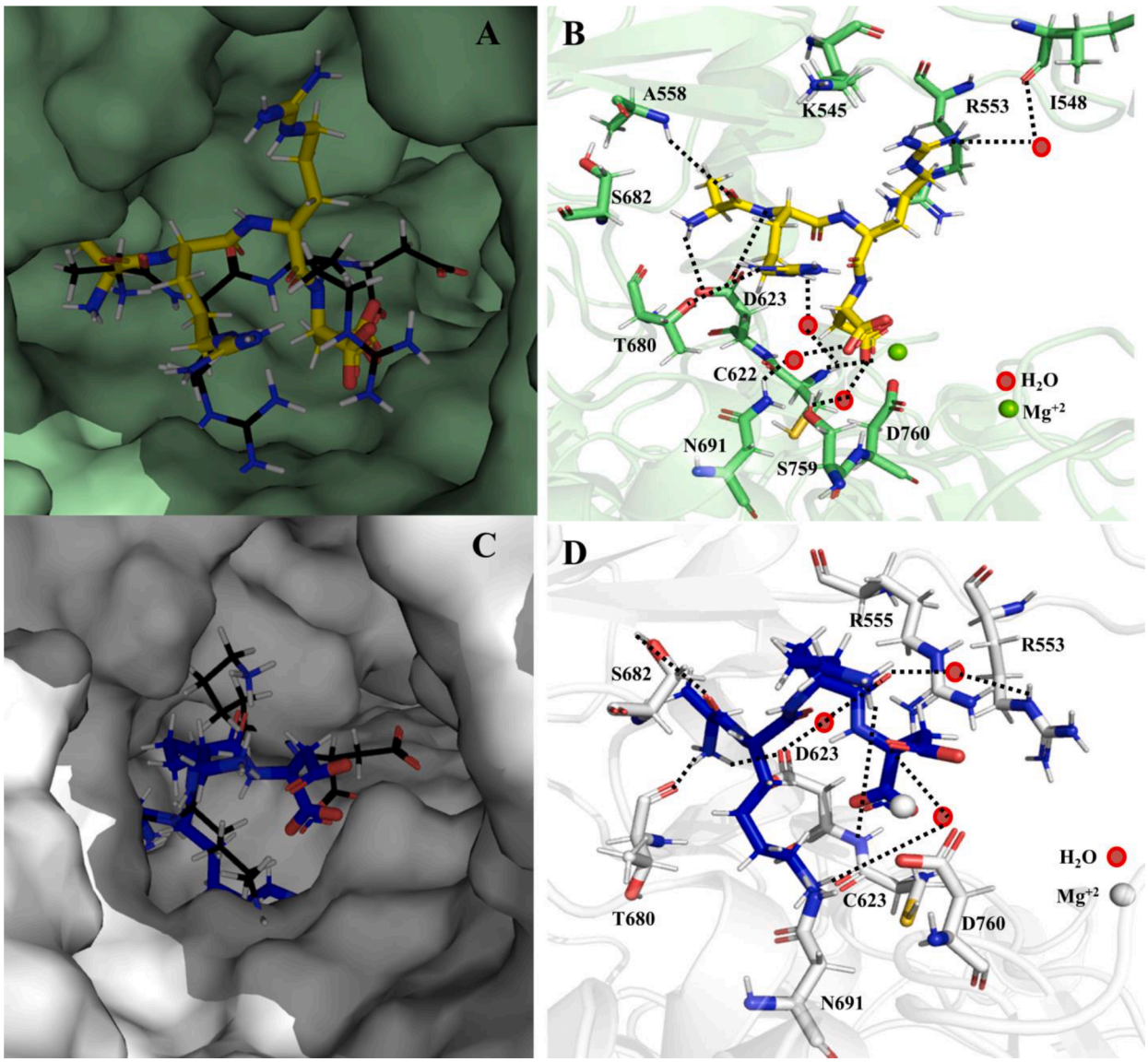

Fig. 6. (A) The comparison of simulated (in pale yellow color) and docked (in black color) conformations of peptide 3 in the active site of the RdRp (surface representation, in pale green color). (B) The average simulated structure of peptide-3-RdRp complex and their various interactions. (C) The comparison of simulated (in blue color) and docked (in black color) conformations of peptide 4 in the active site of the RdRp (surface representation, in white color). D) The average simulated structure of peptide-4-RdRp complex and their various interactions.

unfavorable electrostatic interactions that disfavors its overall binding with RdRp (Fig. 6A,B).

3.2.2. The Binding Mode and Stability of Peptide 4 (Ala1-Lys2-Lys3-Asp4)

Unlike in the case of peptide 2, peptide 4 does not defer too much from its initial docked conformation (Fig. 6C). As a result, it retains some of the initial interactions. It is found that the terminal NH_3^+ group of Ala1 makes an ionic interaction with Asp623 (97% occupancy) and its amide and carbonyl backbone atoms make hydrogen bonds with Asp623 (83% occupancy) and Ser682 (76% occupancy) respectively (Figs. 6D, S11B). Its terminal NH_3^+ group also makes a hydrogen bond with Thr680 (84% occupancy). Similarly, Lys2 makes a hydrogen bond with Cys622 (55% occupancy) and two water-mediated hydrogen bonds with Asp623 and Arg553 (Figs. 6D, S11B). The carbonyl backbone of Lys3 makes a hydrogen bond with Arg555 (30% occupancy), and Asp4 makes ionic interactions with one of the Mg^{+2} ions (100% occupancy). Asp4 also makes water-mediated hydrogen bonds with Asn691 (Figs. 6D, S11B). In addition to these residues, it may also interact with Tyr456, Ala558, Val557, Thr556, Lys545, Met626, Lys676, Thr687, Asp760, etc. (Fig. S8B). Because of the 5 strong interactions (Table 2) and other transient interactions, a ΔG_{bind} of -14.21 kcal/mol is computed for peptide 4-RdRp complex (Table 1). The negative ΔG_{bind} is also because of the non-extension of Lys3 to the binding cleft formed between Arg553 and Arg836 unlike in the case of peptide 3 (Fig. 6A,B). This indicates that peptide 4 would make a very stable complex with RdRp. Further, if we compare both the ΔG_{bind} and the total number of contacts of peptides 2 and 4 with RdRp (Figs. S5B and S8B), it is clear that the latter peptide makes more tight interactions with the protein. The RMSF of binding site residues (residues 400-800) is also less in peptide 4-RdRp complex compared to peptide 2-RdRp complex (Fig. 4B). These results indicate that peptide 4 would act as a promiscuous inhibitor of RdRp.

3.2.3. The Binding Mode and Stability of Peptide 5 (Ala1-Arg2-Lys3-Asp4)

As can be seen from the average simulated complex structure, the initial docked conformation of peptide 5 is almost retained during the simulations (Fig. 7A). In this conformation, Ala1 is not making any interaction with RdRp. However, the terminal NH_2^+ group of Arg2 makes an ionic interaction with Asp623 (97% occupancy) and a

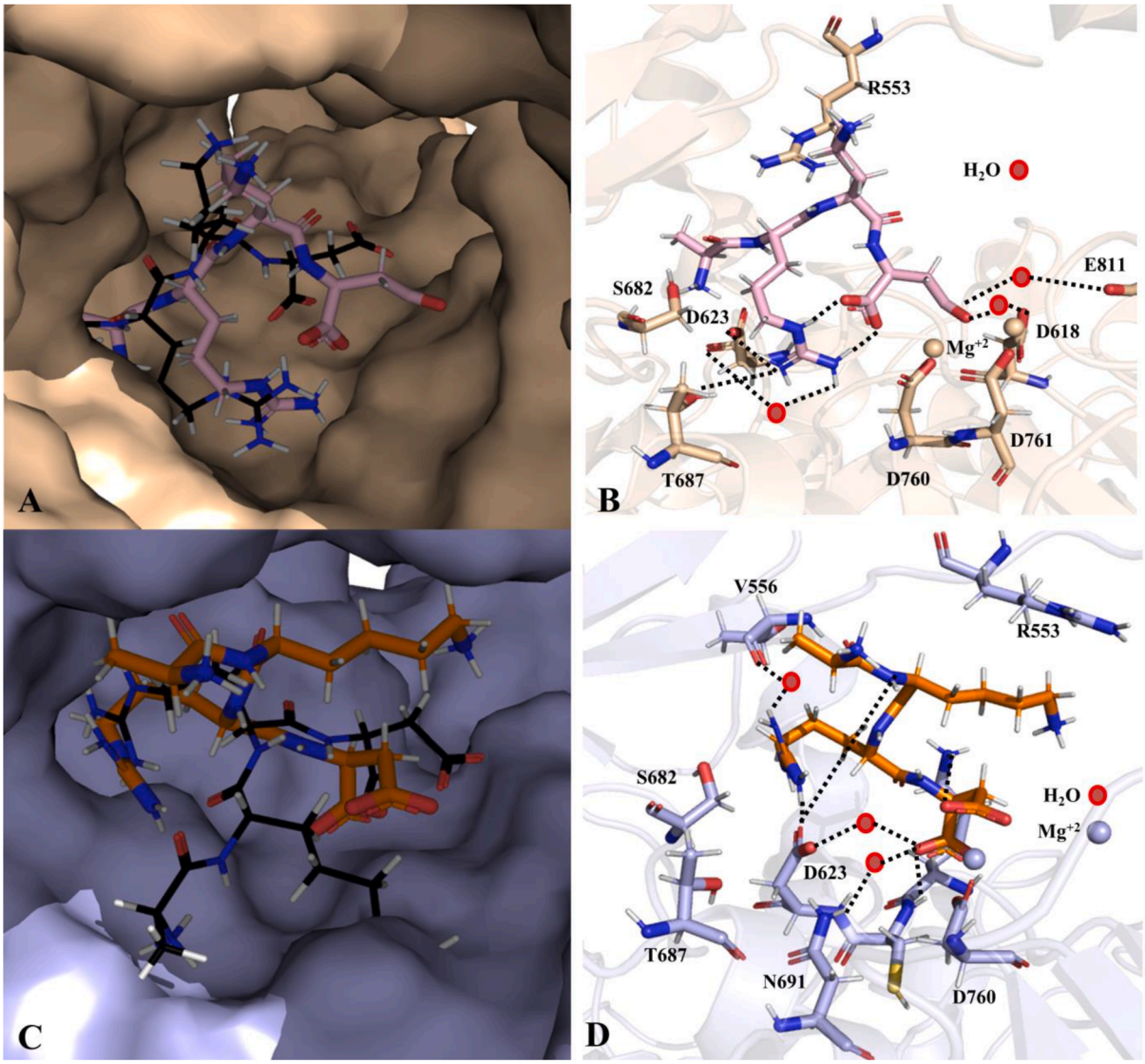

Fig. 7. (A) The comparison of simulated (in light pink color) and docked (in black color) conformations of peptide 5 in the active site of the RdRp (surface representation, in wheat color). (B) The average simulated structure of peptide-5-RdRp complex and their various interactions. (C) The comparison of simulated (in orange color) and docked (in black color) conformations of peptide 6 in the active site of the RdRp (surface representation, in light blue color) D) The average simulated structure of peptide-6-RdRp complex and their various interactions.

hydrogen bond with Thr687 (36% occupancy) (Figs. 7B, S11C). It also makes a water-mediated hydrogen bond with Asp623 (48% occupancy) and two intramolecular hydrogen bonds (more than 90% occupancy) with Asp4 (Figs. 7B, S11C). However, although Asp4 interacted with the Mg^{+2} ion like other peptides, Lys3 failed to interact with RdRp. Asp4 is also found to make water-mediated hydrogen bonds with Asp618 and Glu811 (Figs. 7B, S11C). Other than these residues, peptide 5 may interact with Met452, Tyr455, Tyr456, Thr556, Ala558, Lys545, Arg555, Arg553, Ala547, Ile548, Asp618, Tyr619, Pro620, Lys621, Cys622, Asp623, Arg624, Lys676, Thr680, Ser681, Thr687, Asn691, Ser759, Asp760, Asp761, Glu811, Cys813, S814, Arg836, etc. (Fig. S9A). If we compare the total number of protein-peptide contacts involving peptides 4 and 5 (Figs. S8B and S9A), it is clear that the latter makes more tight interactions with the protein than that of the former. This is also evident from the relative binding free energy data, where a ΔG_{bind} of -17.41 kcal/mol is obtained for the peptide 4-RdRp complex (Table 1). These results imply that the mutation of Lys1 to Arg1 in peptide 4 would enhance its stability and hence inhibitory activities.

3.2.4. *The Binding Mode and Stability of Peptide 6 (Ala1-Lys2-Arg3-Asp4)*

Unlike peptide 5, peptide 6 moved away from its initial docked conformation (Fig. 7C). In the simulated structure, the terminal NH_3^+ group of Ala1 makes one ionic interaction with Asp623 (50% occupancy) and a hydrogen bond with Thr687 (51% occupancy) (Figs. 7D, S11D). However, Lys2 failed to make any interaction with the protein. Interestingly, Arg3 makes a weak salt-bridge interaction (49% occupancy) and a strong hydrogen bond (94% occupancy) with Aps623 (Figs. 7D, S11D). It also makes a weak water-mediated hydrogen bond with Thr556. A weak intramolecular hydrogen bond (30% occupancy) is also formed between the backbone atoms of Arg3 and Lys4. Remarkably, Asp4 is found to make two salt-bridge interactions, one each with one of the Mg^{+2} ions (100% occupancy) and Lys621 (88% occupancy) (Figs. 7D, S11D). It is also found to make a direct hydrogen bond with Cys622 (39% occupancy) and two indirect water-mediated weak hydrogen bonds with Asn691 and Asp623 (Figs. 7D, S11D). Other than these, it can also interact with several other residues as depicted in Fig. S9B. For these reasons, a ΔG_{bind} of -6.28 kcal/mol is obtained for the peptide 6-RdRp complex (Table 1). However, it is about 10 kcal/mol less stable than peptide 5-RdRp complex (Table 1). The suppression of

binding affinity of peptide 6 compared to peptide 5 may be ascribed to (1) fluctuations of the side chains of peptide 6-RdRp complex (Fig. 4C) and (2) unlike peptide 5, Lys2 of peptide 6 is unfavorably placed opposite Arg553. (Fig. 7C). These results indicate that the mutation of Lys3 to Arg3 in peptide 4 would suppress its inhibitory activities.

3.2.5. *The Binding Mode and Stability of Peptide 7 (Arg1-Arg2-Asp3-Asp4)*

Peptide 7 undergoes a significant conformational change during the simulations from its initial docked conformation (Fig. 8A). In this conformation, Arg1 makes two intramolecular hydrogen bonds with Asp3 and its terminal NH_3^+ group makes an ionic interaction with Asp623 (83% occupancy) (Figs. 8B, S12A). Arg2 also makes a salt-bridge interaction (71% occupancy) and a hydrogen bond (73% occupancy) with Asp623. Additionally its amide group makes an intramolecular hydrogen bond with Asp3. However, no protein interaction with Asp3 is formed during the simulations (Figs. 8B, S12A). Remarkably, Asp4 makes ionic interactions with two magnesium ions (Figs. 8B, S12A). Hence, the consideration of two Asp residues at the C-terminal group of the peptide helped it to extend toward the second Mg^{+2} ion, which was observed to bind with the RNA base inserted opposite Remdesivir (Yin et al., 2020). In addition to this, it also makes several water-mediated hydrogen bonds with Tyr619, Cys622, and Asp760 (Figs. 8B, S12A).

For these reasons, a ΔG_{bind} of -10.72 kcal/mol is obtained for the peptide 7-RdRp complex (Table 1). Hence, peptide 7-RdRp complex would be about 7 kcal/mol less stable than the peptide 5-RdRp complex (Table 1). This is quite evident if we compare the total number of protein-peptide contacts involving peptides 5 and 7 (Figs. S9A and S10A).

3.2.6. *The Binding Mode and Stability of Peptide 8 (Asp1-Asp2-Arg3-Lys4)*

During simulations, peptide 8 moved appreciably from its initial docked conformation (Fig. 8C). This is because, instead of interacting with the positive residues of the Finger domains, such as Lys545, Arg553, Arg556, etc., the N-terminal Asp1 moved down to interact with one of the Mg^{+2} ions (Figs. 8D, S12B). In this conformation, its terminal NH_3^+ makes an ionic interaction with Asp618 (69% occupancy), and its carbonyl backbone makes a weak hydrogen bond with Lys545 (33% occupancy) (Figs. 8D, S12B). Except for Asp1, no other residues could make any contact with the protein (Table 2). However, due to the above

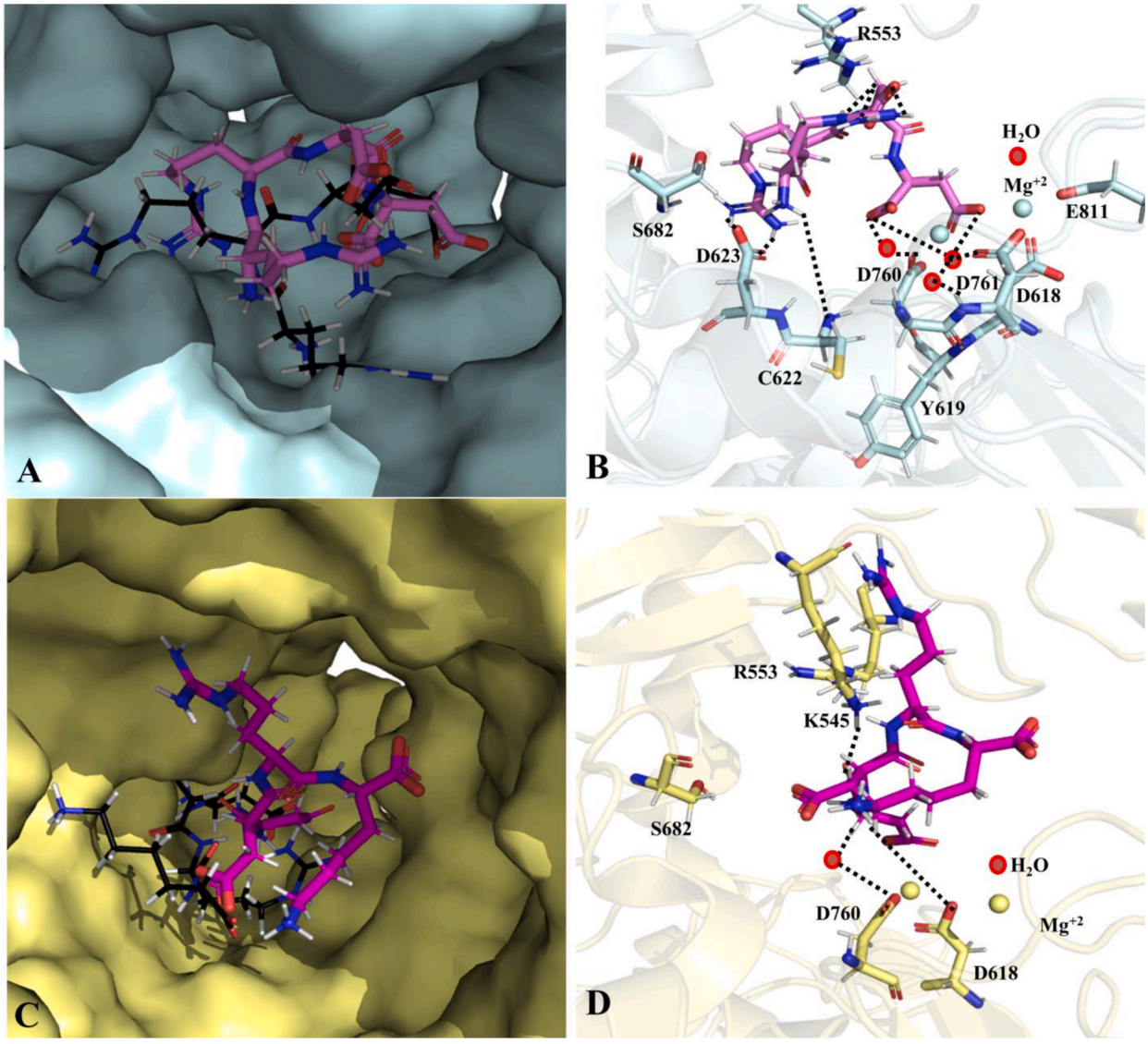

Fig. 8. (A) The comparison of simulated (in violet color) and docked (in black color) conformations of peptide 7 in the active site of the RdRp (surface representation, in pale cyan color) (B) The average simulated structure of peptide-7-RdRp complex and their various interactions. (C) The comparison of simulated (in magenta color) and docked (in black color) conformations of peptide 8 in the active site of the RdRp (surface representation, in pale yellow color) D) The average simulated structure of peptide-8-RdRp complex and their various interactions.

strong electrostatic interactions, a ΔG_{bind} of -10.12 kcal/mol is obtained for the peptide 8-RdRp complex. If we compare ΔG_{bind} of peptide 7-RdRp and peptide 8-RdRp complexes, it is clear that the inhibitory activities of these peptides would be identical. It also indicates that the ability of peptides to bind with RdRp is mainly governed by electrostatic interactions.

4. Domain Movements

As peptide 5-RdRp is associated with the highest ΔG_{bind}, its average structure was superimposed onto the Cryo-EM structure (Yin et al., 2020) to understand the dynamics of different domains after the binding of the peptide inhibitor. The detailed structures are illustrated in Fig. S13. From this Figure, it is clear that the Finger and Thumb domains move significantly during the simulations. As the Finger domain contains the largest number of loops, it is more mobile compared to the Thumb domain. However, the Palm domain remains almost stationary. For example, the side chains of the key residues of the Finger domain that are involved in the inhibitor binding, such as Lys545, Arg555, Arg553, Lys621, Asp623, Arg624, etc. are found to move about 3 to 4Å in the simulated complex. Similarly, the side chains of key residues of the Thumb domain, such as Arg836, Asp845, Arg858, Leu862, etc. are found to move by about 2Å from the observed positions (Yin et al., 2020). Remarkably, the movements of Ser759, Asp760, Asp761, etc. of the Palm domain are found to be marginal (about 0.5-1Å). Interestingly, during the simulations, the metal ions moved toward the Asp760 and Asp761 of the Palm domain to facilitate the inhibitor-metal binding. These results indicate that upon peptide binding, the active site of RdRp becomes more compact and closed.

5. Mechanism of Inhibition

It was recently shown that the i+1 (i refers to the nucleotide insertion site) base of the RNA template strand makes hydrogen bonds with Lys545 and Arg555 of the Finger domain (Yin et al., 2020). Similarly, its backbone was found to make interactions with Ala558, Gly559, Ser682, Gly559, and Gly683. The i-1 and i-2 bases of RNA belonging to the primer strand were observed to make interactions with Asp760, Asp761, Ser759, Cys813, Ser814, and Gln815 (Yin et al., 2020). Remarkably, the purine base of the antiviral drug Remdesivir monophosphate, which was covalently inserted into the NTP site (Yin et al., 2020), was also found to make hydrogen bonds with Lys545 and Arg555. The CN group of its modified sugar was found to make a hydrogen bond with Thr687 and its phosphate groups were found to interact with the Mg^{+2} ions (Yin et al., 2020). Other repurposed nucleotides drugs (Bylehn et al., 2021; Gordon et al., 2021; Sada et al., 2020) and unnatural nucleotides (Jena et al., 2021) were also proposed to bind to the same site.

As peptide inhibitors are found to interact with residues that are involved in making hydrogen bonds with i, i+1, i-1, and i-2 nucleotides of the RNA primer strand (Figs. S14, S15), they would not only block the NTP insertion site but also perturb the RNA primer strand. This would eventually hinder the correct placement of RNA into the active site for nucleotide synthesis. Hence, these inhibitors would inhibit the replication of the viral genome efficiently than those of the nucleotide drugs. Further, unlike nucleotide inhibitors, the inhibition effect would be realized as soon as these inhibitors enter into the NTP site of RdRp and there would be no drug resistance due to the Exon activities. Therefore, it is expected that the peptide inhibitors would be more potent than that of the repurposed nucleotide drugs.

6. Effects of Force Field and Binding Energy Methods

It should be mentioned that consideration of different force fields and binding free energy methods may yield different results. For example, by using the GROMACS 5.1.2 force field and free energy perturbation methods, binding free energy of about -8.0 kcal/mol was computed for the RTP-RdRp complex (Zhang and Zhou, 2020). However, the uses of the ff14SB force field of Amber18 and thermodynamic integration methods had yielded binding free energy of about -35.0 kcal/mol for the RMP-RdRp complex (Bylehn et al., 2021). Similarly, the uses of the OPLS3e force field of Desmond 2018-4 and MM/GBSA method had predicted a positive relative binding free energy for the RMP-RdRp complex (Jena et al., 2021). Although RTP contains three phosphate groups and RMP contains one phosphate group, the purine and sugar groups are the same. Hence, the huge difference in the binding free energies can be ascribed to the methods used in these studies (Bylehn et al., 2021; Jena et al., 2021; Zhang and Zhou, 2020, Jena et al. 2021). However, the comparison of binding modes and relative binding free energies of different inhibitors computed at the same method (e.g. MM/GBSA) can provide useful insights to understand the molecular mechanisms of drug binding and inhibition properties (Genheden and Ryde, 2015). Therefore, if we compare results obtained here with the results obtained for the RMP-RdRp complex by using the MM/GBSA method (Jena et al., 2021), it is likely that the peptide inhibitors having negative binding free energies would be more potent than RMP. Based on ΔG_{bind}, the stabilities and hence the inhibitory activities of these peptides would follow the order: peptide 5> peptide 4> peptide 7≥ peptide 8>peptide 6>peptide 1≥peptide 2≥peptide 3. However, as the ΔG_{bind} values do not include contributions from conformational entropy, they cannot be directly interlinked with the binding constant or IC_{50} values. Further, as the molecular mechanics/generalized Born surface area method (MM/GBSA) is less accurate compared to the molecular mechanics/Poisson-Boltzman surface area method (MM/PBSA), results obtained at the former method are less reliable than that of the later method (Hou et al., 2011).

Similarly, it is also not reliable to use docking scores to rank the inhibition abilities of these peptide inhibitors. This is because not only docking algorithms are based on empirical parameters but also they do not account for solvation effects, protein reorganization, and dynamics. For example, as per the docking results, peptides 4 and 5 are the least stable, while they are the most stable as per the MM/GBSA results (Table 1). Therefore, experimental structural studies and evaluations of bioactivity and biosafety of the RdRp-peptide complexes studied herein would yield more interesting results.

It should be mentioned that the use of similar short peptide inhibitors against several flaviviruses is found to be very effective and safe. It was shown that the use of di- or tri- or tetrapeptide analogs can inhibit flaviviruses, such as DENV, WNV, and ZKV with affinities in the micromolar to nanomolar ranges (Nitsche et al., 2017). For example, the affinities of a dipeptide Bz-(4-guanidino)Phe-Arg-$B(OH)_2$ (binding constant (K_i) = 0.027 μM) (Nitsche et al., 2017) and tetrapeptide Bz-Nle--Lys-Arg-Arg-$B(OH)_2$ (K_i = 0.043 μM) (Schuller et al., 2011) inhibitors against DENV protease were in the micromolar range. Similarly, for a tripeptide Bz-Arg-Lys-X-NH_2 (X=4-(Benzyloxy)-D-phenyl glycine) with C- and N-terminal modifications by 4-CF_3-benzyl ether and thiazole respectively produced IC_{50} values of 18 nM (K_i=12 nM) and 50 nM (K_i=39 nM) for the inhibition of DNV and WNV respectively (Behnam et al., 2015). These results indicate that peptide inhibitors can bind strongly to the active sites of the proteases. Based on these results, it can be proposed that the potencies of peptides 4 and 5 in inhibiting RdRp would be similar to the above peptides (Behnam et al., 2015; Nitsche et al., 2017; Schuller et al., 2011).

Conclusions

It is revealed that the electrostatically active binding site of the RdRp can be inhibited by designing short ionic peptide inhibitors that may make direct or indirect interactions with different active site residues of RdRp. Based on dynamics and relative binding free energies (ΔG_{bind}), the efficiency of peptide inhibitors can be categorized into mainly three parts, namely (1) highly efficient, (2) moderately efficient, and (3) poorly efficient. For example, as the ΔG_{bind} of RdRp-peptide 4 and RdRp-

peptide 5 complexes are -14.21 and -17.41 kcal/mol respectively, peptides 4 and 5 would be highly efficient in inhibiting the RdRp activities. Similarly, peptides 6 to 8, whose ΔG_{bind} lie between ~-6 to -10 kcal/mol, would possess moderate inhibitory activities, while peptides 1 to 3 may possess lower inhibitory activities. As peptides 4 to 8 are of four amino acids long, it can be proposed that tetrapeptides would be more effective than that of tripeptides in inhibiting RdRp activities. It is further revealed that these inhibitors would block the NTP insertion site of RdRp, thereby obstructing the insertions of new nucleotides into the RNA strand. This would eventually block the replication of the viral gene. However, experimental structural evaluations, and determinations of *in vivo* activities, such as bioactivity, safety, and membrane permeability of these peptide inhibitors would provide more interesting insights. Nevertheless, this study for the first time has demonstrated that peptide inhibitors may act as attractive drug candidates against COVID-19 and there is a tremendous potential to design even more potent peptide inhibitors by either changing sequences or adding small molecules at the C- and N-terminals.

Credit Statements

Both the authors have equally contributed to this work.

Conflict of Interest

There are no conflicts of interest to declare.

Acknowledgments

NRJ is thankful to the Science and Engineering Research Board (SERB), Department of Science and Technology (DST, New-Delhi), and the Council of Scientific and Industrial Research (CSIR, NewDelhi) for financial supports. SP is thankful to NIPER, Kolkata, and the Department of Pharmaceuticals, Ministry of Chemicals and Fertilizers, Government of India, for providing necessary resources and fellowship. We acknowledge the contributions of the late Dr. Hemant Kumar Srivastava to this article and want to dedicate this work to his memory.

Supplementary materials

Supplementary material associated with this article can be found, in the online version, at doi:10.1016/j.ejps.2021.106012.

References

Astuti, I., Ysrafil, 2020. Severe Acute Respiratory Syndrome Coronavirus 2 (SARS-CoV-2): An overview of viral structure and host response. Diabetes & metabolic syndrome 14, 407–412.

Behnam, M.A., Graf, D., Bartenschlager, R., Zlotos, D.P., Klein, C.D., 2015. Discovery of Nanomolar Dengue and West Nile Virus Protease Inhibitors Containing a 4-Benzyloxyphenylglycine Residue. Journal of medicinal chemistry 58, 9354–9370.

Berendsen, H.J.C., Grigera, J.R., Straatsma, T.P., 1987. The missing term in effective pair potentials. The Journal of Physical Chemistry 91, 6269–6271.

Bowers, K.J., Chow, D.E., Xu, H., Dror, R.O., Eastwood, M.P., Gregersen, B.A., Klepeis, J. L., Kolossvary, I., Moraes, M.A., Sacerdoti, F.D., Salmon, J.K., Shan, Y., Shaw, D.E., 2006a. In: Scalable Algorithms for Molecular Dynamics Simulations on Commodity Clusters, SC '06: Proceedings of the 2006 ACM/IEEE Conference on Supercomputing, 43-43.

Bowers, K.J., Chow, E., Xu, H., Dror, R.O., Eastwood, M.P., Gregersen, B.A., Klepeis, J.L., Kolossvary, I., Moraes, M.A., Sacerdoti, F.D., Salmon, J.K., Shan, Y., Shaw, D.E., 2006b. Scalable algorithms for molecular dynamics simulations on commodity clusters. In: Proceedings of the 2006 ACM/IEEE conference on Supercomputing. Tampa, Florida. Association for Computing Machinery, pp. 84–es.

Buchholz, U.J., Bukreyev, A., Yang, L., Lamirande, E.W., Murphy, B.R., Subbarao, K., Collins, P.L., 2004. Contributions of the structural proteins of severe acute respiratory syndrome coronavirus to protective immunity. In: Proceedings of the National Academy of Sciences of the United States of America, 101, pp. 9804–9809.

Bylehn, F., Menendez, C.A., Perez-Lemus, G.R., Alvarado, W., de, Pablo, J.J., 2021. Modeling the Binding Mechanism of Remdesivir, Favilavir, and Ribavirin to SARS-CoV-2 RNA-Dependent RNA Polymerase. ACS central science 7, 164–174.

Cava, C., Bertoli, G., Castiglioni, I., 2020. Silico Discovery of Candidate Drugs against Covid-19. Viruses 12.

Chowdhury, S.M., Talukder, S.A., Khan, A.M., Afrin, N., Ali, M.A., Islam, R., Parves, R., Al Mamun, A., Sufian, M.A., Hossain, M.N., Hossain, M.A., Halim, M.A., 2020. Antiviral Peptides as Promising Therapeutics against SARS-CoV-2. The journal of physical chemistry B 124, 9785–9792.

da Silva, S.J.R., Alves da Silva, C.T., Mendes, R.P.G., Pena, L., 2020. Role of nonstructural proteins in the pathogenesis of SARS-CoV-2. Journal of medical virology 92, 1427–1429.

Gahtori, J., Pant, S., Srivastava, H.K., 2020. Modeling antimalarial and antihuman African trypanosomiasis compounds: a ligand- and structure-based approaches. Molecular diversity 24, 1107–1124.

Gao, Y., Yan, L., Huang, Y., Liu, F., Zhao, Y., Cao, L., Wang, T., Sun, Q., Ming, Z., Zhang, L., Ge, J., Zheng, L., Zhang, Y., Wang, H., Zhu, Y., Zhu, C., Hu, T., Hua, T., Zhang, B., Yang, X., Li, J., Yang, H., Liu, Z., Xu, W., Guddat, L.W., Wang, Q., Lou, Z., Rao, Z., 2020. Structure of the RNA-dependent RNA polymerase from COVID-19 virus. Science 368, 779–782.

Genheden, S., Ryde, U., 2015. The MM/PBSA and MM/GBSA methods to estimate ligand-binding affinities. Expert opinion on drug discovery 10, 449–461.

Gomara, M.J., Perez, Y., Gomez-Gutierrez, P., Herrera, C., Ziprin, P., Martinez, J.P., Meyerhans, A., Perez, J.J., Haro, I., 2020. Importance of structure-based studies for the design of a novel HIV-1 inhibitor peptide. Scientific reports 10, 14430.

Gordon, C.J., Tchesnokov, E.P., Schinazi, R.F., Gotte, M., 2021. Molnupiravir promotes SARS-CoV-2 mutagenesis via the RNA template. The Journal of biological chemistry 297, 100770.

Gordon, C.J., Tchesnokov, E.P., Woolner, E., Perry, J.K., Feng, J.Y., Porter, D.P., Gotte, M., 2020. Remdesivir is a direct-acting antiviral that inhibits RNA-dependent RNA polymerase from severe acute respiratory syndrome coronavirus 2 with high potency. The Journal of biological chemistry 295, 6785–6797.

Hartshorn, M.J., Verdonk, M.L., Chessari, G., Brewerton, S.C., Mooij, W.T., Mortenson, P. N., Murray, C.W., 2007. Diverse, high-quality test set for the validation of protein-ligand docking performance. Journal of medicinal chemistry 50, 726–741.

Hou, T., Wang, J., Li, Y., Wang, W., 2011. Assessing the performance of the MM/PBSA and MM/GBSA methods. 1. The accuracy of binding free energy calculations based on molecular dynamics simulations. Journal of chemical information and modeling 51, 69–82.

Jena, N., 2020a. ChemRxiv Preprint.

Jena, N.R., 2020b. Role of different tautomers in the base-pairing abilities of some of the vital antiviral drugs used against COVID-19. Physical chemistry chemical physics: PCCP 22, 28115–28122.

Jena, N.R., 2021. Drug targets, mechanisms of drug action, and therapeutics against SARS-CoV-2. Chemical Physics Impact 2, 100011.

Jena, N.R., Pant, S., Srivastava, H.K., 2021. Artificially expanded genetic information systems (AEGISs) as potent inhibitors of the RNA-dependent RNA polymerase of the SARS-CoV-2. Journal of biomolecular structure & dynamics 1–17.

Jones, G., Willett, P., Glen, R.C., Leach, A.R., Taylor, R., 1997. Development and validation of a genetic algorithm for flexible docking. Journal of molecular biology 267, 727–748.

Kadam, R.U., Wilson, I.A., 2017. Structural basis of influenza virus fusion inhibition by the antiviral drug Arbidol. In: Proceedings of the National Academy of Sciences of the United States of America, 114, pp. 206–214.

Lan, J., Ge, J., Yu, J., Shan, S., Zhou, H., Fan, S., Zhang, Q., Shi, X., Wang, Q., Zhang, L., Wang, X., 2020. Structure of the SARS-CoV-2 spike receptor-binding domain bound to the ACE2 receptor. Nature 581, 215–220.

Li, G., De Clercq, E., 2020. Therapeutic options for the 2019 novel coronavirus (2019-nCoV). Nature reviews. Drug discovery 19, 149–150.

Li, Y., Han, L., Liu, Z., Wang, R., 2014. Comparative assessment of scoring functions on an updated benchmark: 2. Evaluation methods and general results. Journal of chemical information and modeling 54, 1717–1736.

Li, Y., Xie, Z., Lin, W., Cai, W., Wen, C., Guan, Y., Mo, X., Wang, J., Wang, Y., Peng, P., Chen, X., Hong, W., Xiao, G., Liu, J., Zhang, L., Hu, F., Li, F., Zhang, F., Deng, X., Li, L., 2020. Efficacy and Safety of Lopinavir/Ritonavir or Arbidol in Adult Patients with Mild/Moderate COVID-19: An Exploratory Randomized Controlled Trial. Med 1, 105–113 e104.

Liu, C., Shi, W., Becker, S.T., Schatz, D.G., Liu, B., Yang, Y., 2021. Structural basis of mismatch recognition by a SARS-CoV-2 proofreading enzyme. Science.

Liu, C., Zhou, Q., Li, Y., Garner, L.V., Watkins, S.P., Carter, L.J., Smoot, J., Gregg, A.C., Daniels, A.D., Jervey, S., Albaiu, D., 2020. Research and Development on Therapeutic Agents and Vaccines for COVID-19 and Related Human Coronavirus Diseases. ACS central science 6, 315–331.

Martyna, G.J., Tobias, D.J., Klein, M.L., 1994. Constant pressure molecular dynamics algorithms. The Journal of chemical physics 101, 4177–4189.

Morris, J.H., Huang, C.C., Babbitt, P.C., Ferrin, T.E., 2007. structureViz: linking Cytoscape and UCSF Chimera. Bioinformatics 23, 2345–2347.

Nissink, J.W., Murray, C., Hartshorn, M., Verdonk, M.L., Cole, J.C., Taylor, R., 2002. A new test set for validating predictions of protein-ligand interaction. Proteins 49, 457–471.

Nitsche, C., Zhang, L., Weigel, L.F., Schilz, J., Graf, D., Bartenschlager, R., Hilgenfeld, R., Klein, C.D., 2017. Peptide-Boronic Acid Inhibitors of Flaviviral Proteases: Medicinal Chemistry and Structural Biology. Journal of medicinal chemistry 60, 511–516.

Noble, C.G., Seh, C.C., Chao, A.T., Shi, P.Y., 2012. Ligand-bound structures of the dengue virus protease reveal the active conformation. Journal of virology 86, 438–446.

Pant, S., Singh, M., Ravichandiran, V., Murty, U.S.N., Srivastava, H.K., 2021. Peptide-like and small-molecule inhibitors against Covid-19. Journal of biomolecular structure & dynamics 39, 2904–2913.

Phoo, W.W., Zhang, Z., Wirawan, M., Chew, E.J.C., Chew, A.B.L., Kouretova, J., Steinmetzer, T., Luo, D., 2018. Structures of Zika virus NS2B-NS3 protease in complex with peptidomimetic inhibitors. Antiviral research 160, 17–24.

Posch, H.A., Hoover, W.G., Vesely, F.J., 1986. Canonical dynamics of the Nose oscillator: Stability, order, and chaos. Physical review. A, General physics 33, 4253–4265.
Roos, K., Wu, C., Damm, W., Reboul, M., Stevenson, J.M., Lu, C., Dahlgren, M.K., Mondal, S., Chen, W., Wang, L., Abel, R., Friesner, R.A., Harder, E.D., 2019. OPLS3e: Extending Force Field Coverage for Drug-Like Small Molecules. Journal of chemical theory and computation 15, 1863–1874.
Sada, M., Saraya, T., Ishii, H., Okayama, K., Hayashi, Y., Tsugawa, T., Nishina, A., Murakami, K., Kuroda, M., Ryo, A., Kimura, H., 2020. Detailed Molecular Interactions of Favipiravir with SARS-CoV-2, SARS-CoV, MERS-CoV, and Influenza Virus Polymerases In Silico. Microorganisms 8.
Sapundzhi, F., Prodanova, K., Lazarova, M., 2019. Survey of the scoring functions for protein-ligand docking. AIP Conference Proceedings 2172, 100008.
Schrödinger, L., 2015. The PyMOL Molecular Graphics System.
Schuller, A., Yin, Z., Brian Chia, C.S., Doan, D.N., Kim, H.K., Shang, L., Loh, T.P., Hill, J., Vasudevan, S.G., 2011. Tripeptide inhibitors of dengue and West Nile virus NS2B-NS3 protease. Antiviral research 92, 96–101.
Schutz, D., Ruiz-Blanco, Y.B., Munch, J., Kirchhoff, F., Sanchez-Garcia, E., Muller, J.A., 2020. Peptide and peptide-based inhibitors of SARS-CoV-2 entry. Advanced drug delivery reviews 167, 47–65.
Sheahan, T.P., Sims, A.C., Leist, S.R., Schafer, A., Won, J., Brown, A.J., Montgomery, S. A., Hogg, A., Babusis, D., Clarke, M.O., Spahn, J.E., Bauer, L., Sellers, S., Porter, D., Feng, J.Y., Cihlar, T., Jordan, R., Denison, M.R., Baric, R.S., 2020. Comparative therapeutic efficacy of remdesivir and combination lopinavir, ritonavir, and interferon beta against MERS-CoV. Nature communications 11, 222.
Snijder, E.J., Decroly, E., Ziebuhr, J., 2016. The Nonstructural Proteins Directing Coronavirus RNA Synthesis and Processing. Advances in virus research 96, 59–126.
Ullah, H., Ullah, A., Gul, A., Mousavi, T., Khan, M.W., 2021. Novel coronavirus 2019 (COVID-19) pandemic outbreak: A comprehensive review of the current literature. Vacunas 22, 106–113.
Walls, A.C., Park, Y.J., Tortorici, M.A., Wall, A., McGuire, A.T., Veesler, D., 2020. Structure, Function, and Antigenicity of the SARS-CoV-2 Spike Glycoprotein. Cell 181, 281–292 e286.
Wang, D., Hu, B., Hu, C., Zhu, F., Liu, X., Zhang, J., Wang, B., Xiang, H., Cheng, Z., Xiong, Y., Zhao, Y., Li, Y., Wang, X., Peng, Z., 2020. Clinical Characteristics of 138 Hospitalized Patients With 2019 Novel Coronavirus-Infected Pneumonia in Wuhan. China. Jama 323, 1061–1069.
Weng, G., Gao, J., Wang, Z., Wang, E., Hu, X., Yao, X., Cao, D., Hou, T., 2020. Comprehensive Evaluation of Fourteen Docking Programs on Protein-Peptide Complexes. Journal of chemical theory and computation 16, 3959–3969.
Wu, R., Wang, L., Kuo, H.D., Shannar, A., Peter, R., Chou, P.J., Li, S., Hudlikar, R., Liu, X., Liu, Z., Poiani, G.J., Amorosa, L., Brunetti, L., Kong, A.N., 2020. An Update on Current Therapeutic Drugs Treating COVID-19. Current pharmacology reports 1–15.
Yin, W., Mao, C., Luan, X., Shen, D.D., Shen, Q., Su, H., Wang, X., Zhou, F., Zhao, W., Gao, M., Chang, S., Xie, Y.C., Tian, G., Jiang, H.W., Tao, S.C., Shen, J., Jiang, Y., Jiang, H., Xu, Y., Zhang, S., Zhang, Y., Xu, H.E., 2020. Structural basis for inhibition of the RNA-dependent RNA polymerase from SARS-CoV-2 by remdesivir. Science 368, 1499–1504.
Zhang, L., Zhou, R., 2020. Structural Basis of the Potential Binding Mechanism of Remdesivir to SARS-CoV-2 RNA-Dependent RNA Polymerase. The journal of physical chemistry. B 124, 6955–6962.
Zhou, Y., Hou, Y., Shen, J., Huang, Y., Martin, W., Cheng, F., 2020. Network-based drug repurposing for novel coronavirus 2019-nCoV/SARS-CoV-2. Cell discovery 6, 14.